The Astrophysical Journal, 975:5 (12pp), 2024 November 1 https://doi.org/10.3847/1538-4357/ad739a

The Dark Energy Survey Supernova Program: Light Curves and 5 Yr Data Release

B. O. Sánchez[1,2], D. Brout[3], M. Vincenzi[2], M. Sako[4], K. Herner[5], R. Kessler[6,7], T. M. Davis[8], D. Scolnic[2], M. Acevedo[2], J. Lee[4], A. Möller[9], H. Qu[4], L. Kelsey[10], P. Wiseman[11], P. Armstrong[12], B. Rose[2,13], R. Camilleri[8], R. Chen[2], L. Galbany[14,15], E. Kovacs[16], C. Lidman[12,17], B. Popovic[2,18], M. Smith[19], P. Shah[20], M. Sullivan[11], M. Toy[11], T. M. C. Abbott[21], M. Aguena[22], S. Allam[5], O. Alves[23], J. Annis[5], J. Asorey[24], S. Avila[25], D. Bacon[10], D. Brooks[20], D. L. Burke[26,27], A. Carnero Rosell[22,28], D. Carollo[29], J. Carretero[25], L. N. da Costa[22], F. J. Castander[14,15], S. Desai[30], H. T. Diehl[5], J. Duarte[31], S. Everett[32], I. Ferrero[33], B. Flaugher[5], J. Frieman[5,7], J. García-Bellido[34], M. Gatti[4], E. Gaztanaga[10,14,15], G. Giannini[7,25], K. Glazebrook[9], S. González-Gaitán[31], R. A. Gruendl[35,36], G. Gutierrez[5], S. R. Hinton[8], D. L. Hollowood[37], K. Honscheid[38,39], D. J. James[40], K. Kuehn[41,42], O. Lahav[20], S. Lee[32], G. F. Lewis[43], H. Lin[5], J. L. Marshall[44], J. Mena-Fernández[45], R. Miquel[25,46], J. Myles[47], R. C. Nichol[48], R. L. C. Ogando[49], A. Palmese[50], M. E. S. Pereira[51], A. Pieres[22,49], A. A. Plazas Malagón[26,27], A. Porredon[52], A. K. Romer[53], E. Sanchez[54], D. Sanchez Cid[54], I. Sevilla-Noarbe[54], E. Suchyta[55], M. E. C. Swanson[35], G. Tarle[23], B. E. Tucker[12], D. L. Tucker[5], V. Vikram[56], A. R. Walker[21], and N. Weaverdyck[57,58]
(DES Collaboration)

[1] Aix Marseille Univ, CNRS/IN2P3, CPPM, Marseille, France; bsanchez@cppm.in2p3.fr
[2] Department of Physics, Duke University, Durham, NC 27708, USA
[3] Departments of Astronomy and Physics, Boston University, Boston, MA 02140, USA
[4] Department of Physics and Astronomy, University of Pennsylvania, Philadelphia, PA 19104, USA
[5] Fermi National Accelerator Laboratory, P.O. Box 500, Batavia, IL 60510, USA
[6] Department of Astronomy and Astrophysics, University of Chicago, Chicago, IL 60637, USA
[7] Kavli Institute for Cosmological Physics, University of Chicago, Chicago, IL 60637, USA
[8] School of Mathematics and Physics, University of Queensland, Brisbane, QLD 4072, Australia
[9] Centre for Astrophysics & Supercomputing, Swinburne University of Technology, Victoria 3122, Australia
[10] Institute of Cosmology and Gravitation, University of Portsmouth, Portsmouth PO1 3FX, UK
[11] School of Physics and Astronomy, University of Southampton, Southampton SO17 1BJ, UK
[12] The Research School of Astronomy and Astrophysics, Australian National University, ACT 2601, Australia
[13] Department of Physics, Baylor University, One Bear Place #97316, Waco, TX 76798-7316, USA
[14] Institut d'Estudis Espacials de Catalunya (IEEC), 08034 Barcelona, Spain
[15] Institute of Space Sciences (ICE, CSIC), Campus UAB, Carrer de Can Magrans, 08193 Barcelona, Spain
[16] Argonne National Laboratory, 9700 South Cass Avenue, Lemont, IL 60439, USA
[17] Centre for Gravitational Astrophysics, College of Science, The Australian National University, ACT 2601, Australia
[18] University of Lyon, Univ Claude Bernard Lyon 1, CNRS, IP2I Lyon/IN2P3, IMR 5822, F-69622 Villeurbanne, France
[19] Physics Department, Lancaster University, Lancaster LA1 4YB, UK
[20] Department of Physics & Astronomy, University College London, Gower Street, London WC1E 6BT, UK
[21] Cerro Tololo Inter-American Observatory, NSF's National Optical-Infrared Astronomy Research Laboratory, Casilla 603, La Serena, Chile
[22] Laboratório Interinstitucional de e-Astronomia—LIneA, Rua Gal. José Cristino 77, Rio de Janeiro, RJ 20921-400, Brazil
[23] Department of Physics, University of Michigan, Ann Arbor, MI 48109, USA
[24] Departamento de Física Teórica and IPARCOS, Universidad Complutense de Madrid, 28040 Madrid, Spain
[25] Institut de Física d'Altes Energies (IFAE), The Barcelona Institute of Science and Technology, Campus UAB, 08193 Bellaterra (Barcelona), Spain
[26] Kavli Institute for Particle Astrophysics & Cosmology, P.O. Box 2450, Stanford University, Stanford, CA 94305, USA
[27] SLAC National Accelerator Laboratory, Menlo Park, CA 94025, USA
[28] Instituto de Astrofisica de Canarias, E-38205 La Laguna, Tenerife, Spain
[29] INAF-Osservatorio Astronomico di Trieste, via G. B. Tiepolo 11, I-34143 Trieste, Italy
[30] Department of Physics, IIT Hyderabad, Kandi, Telangana 502285, India
[31] CENTRA, Instituto Superior Técnico, Universidade de Lisboa, Av. Rovisco Pais 1, 1049-001 Lisboa, Portugal
[32] Jet Propulsion Laboratory, California Institute of Technology, 4800 Oak Grove Drive, Pasadena, CA 91109, USA
[33] Institute of Theoretical Astrophysics, University of Oslo, P.O. Box 1029, Blindern, NO-0315 Oslo, Norway
[34] Instituto de Fisica Teorica UAM/CSIC, Universidad Autonoma de Madrid, 28049 Madrid, Spain
[35] Center for Astrophysical Surveys, National Center for Supercomputing Applications, 1205 West Clark St., Urbana, IL 61801, USA
[36] Department of Astronomy, University of Illinois at Urbana-Champaign, 1002 W. Green Street, Urbana, IL 61801, USA
[37] Santa Cruz Institute for Particle Physics, Santa Cruz, CA 95064, USA
[38] Center for Cosmology and Astro-Particle Physics, The Ohio State University, Columbus, OH 43210, USA
[39] Department of Physics, The Ohio State University, Columbus, OH 43210, USA
[40] Center for Astrophysics | Harvard & Smithsonian, 60 Garden Street, Cambridge, MA 02138, USA
[41] Australian Astronomical Optics, Macquarie University, North Ryde, NSW 2113, Australia
[42] Lowell Observatory, 1400 Mars Hill Rd, Flagstaff, AZ 86001, USA
[43] Sydney Institute for Astronomy, School of Physics, A28, The University of Sydney, NSW 2006, Australia
[44] George P. and Cynthia Woods Mitchell Institute for Fundamental Physics and Astronomy, and Department of Physics and Astronomy, Texas A&M University, College Station, TX 77843, USA
[45] LPSC Grenoble—53, Avenue des Martyrs, 38026 Grenoble, France
[46] Institució Catalana de Recerca i Estudis Avançats, E-08010 Barcelona, Spain
[47] Department of Astrophysical Sciences, Princeton University, Peyton Hall, Princeton, NJ 08544, USA
[48] School of Mathematics and Physics, University of Surrey, Guildford, Surrey GU2 7XH, UK
[49] Observatório Nacional, Rua Gal. José Cristino 77, Rio de Janeiro, RJ 20921-400, Brazil
[50] Department of Physics, Carnegie Mellon University, Pittsburgh, PA 15312, USA
[51] Hamburger Sternwarte, Universität Hamburg, Gojenbergsweg 112, 21029 Hamburg, Germany
[52] Ruhr University Bochum, Faculty of Physics and Astronomy, Astronomical Institute, German Centre for Cosmological Lensing, 44780 Bochum, Germany
[53] Department of Physics and Astronomy, Pevensey Building, University of Sussex, Brighton BN1 9QH, UK

[54] Centro de Investigaciones Energéticas, Medioambientales y Tecnológicas (CIEMAT), Madrid, Spain
[55] Computer Science and Mathematics Division, Oak Ridge National Laboratory, Oak Ridge, TN 37831, USA
[56] Argonne National Laboratory, 9700 S Cass Avenue, Lemont, IL 60439, USA
[57] Department of Astronomy, University of California, Berkeley, 501 Campbell Hall, Berkeley, CA 94720, USA
[58] Lawrence Berkeley National Laboratory, 1 Cyclotron Road, Berkeley, CA 94720, USA
Received 2024 July 3; revised 2024 August 22; accepted 2024 August 23; published 2024 October 21

Abstract

We present *griz* photometric light curves for the full 5 yr of the Dark Energy Survey Supernova (DES-SN) program, obtained with both forced point-spread function photometry on difference images (`DiffImg`) performed during survey operations, and scene modelling photometry (SMP) on search images processed after the survey. This release contains 31,636 `DiffImg` and 19,706 high-quality SMP light curves, the latter of which contain 1635 photometrically classified SNe that pass cosmology quality cuts. This sample spans the largest redshift (z) range ever covered by a single SN survey ($0.1 < z < 1.13$) and is the largest single sample from a single instrument of SNe ever used for cosmological constraints. We describe in detail the improvements made to obtain the final DES-SN photometry and provide a comparison to what was used in the 3 yr DES-SN spectroscopically confirmed Type Ia SN sample. We also include a comparative analysis of the performance of the SMP photometry with respect to the real-time `DiffImg` forced photometry and find that SMP photometry is more precise, more accurate, and less sensitive to the host-galaxy surface brightness anomaly. The public release of the light curves and ancillary data can be found at github.com/des-science/DES-SN5YR and doi:10.5281/zenodo.12720777.

Unified Astronomy Thesaurus concepts: Cosmology (343); Type Ia supernovae (1728); Dark energy (351)

1. Introduction

Type Ia Supernovae (SNe Ia) are an established cosmological probe, used to discover the accelerating expansion of the Universe (A. G. Riess et al. 1998; S. Perlmutter et al. 1999), and constrain the dark energy equation of state parameter, w. The Dark Energy Survey (DES), conceived in the period following the discovery of the accelerating Universe, has completed a 5 yr SN Ia discovery and follow-up program (DES-SN) using repeated (1 week cadence) observations of 27 deg^2 with the Dark Energy Camera (DECam; B. Flaugher et al. 2015) at the Cerro Tololo International Observatory starting in 2013 August and ending in 2018 January. It has assembled the largest sample of SNe Ia ever observed with a single instrument with 1635 photometrically classified SNe Ia suitable for cosmology over the redshift interval $0.1 < z < 1.13$.

A first set of cosmology results using only the first 3 yr (DES-SN3YR) of spectroscopically confirmed SNe Ia was released in 2019 (D. Brout et al. 2019b, 2019b; T. M. C. Abbott et al. 2019; M. Smith et al. 2020), including a total of 251 light curves. The purpose of this first analysis was to provide competitive constraints, to spur the development of key data processing and analysis pipelines, and also to identify areas for improvement. The tools for the 5 yr analysis were developed over many years and are reported in a number of papers. These software tools include difference imaging (`DiffImg`; R. Kessler et al. 2015), scene modeling photometry (SMP; D. Brout et al. 2019a), chromatic corrections (D. L. Burke et al. 2018; J. Lasker et al. 2019), simulated bias corrections (R. Kessler et al. 2019, hereafter K19), host-mass correlations (M. Smith et al. 2020; L. Kelsey et al. 2021, 2023), photometric classification (M. Vincenzi et al. 2019; A. Moller & T. de'Boissiere 2020; A. Moller et al. 2022), and a comprehensive analysis framework (R. Kessler et al. 2009, SNANA K09; S. Hinton & D. Brout 2020, Pippin; D. Brout et al. 2021; P. Armstrong et al. 2023; R. Kessler et al. 2023; H. Qu et al. 2024). The complete analysis using these software tools is presented in M. Vincenzi et al. (2024) and DES Collaboration (2024).

For the 5 yr analysis, DES has compiled a sample of photometrically classified SNe Ia that is an order of magnitude larger than that used in the spectroscopically classified DES-SN3YR analysis. This larger sample, hereafter DES-SN5YR, has resulted in a 30% reduction in statistical uncertainties in the dark energy equation of state parameter, w, with respect to the initial DES-SN3YR analysis (D. Brout et al. 2019b; T. M. C. Abbott et al. 2019; DES Collaboration 2024; M. Vincenzi et al. 2024). The uncertainty reduction is less than the naive $\sqrt{N_{\rm SNe}}$ because (i) the number of spectroscopically confirmed low-redshift events is similar to that in the 3 yr analysis, (ii) the cosmic microwave background (CMB) constraint is only slightly improved w.r.t. the 3 yr analysis, and (iii) the additional events with photometric classification tend to have a lower signal-to-noise ratio (SNR) compared to the spectroscopically confirmed sample. However, along with smaller statistical uncertainties comes an increased need to reduce systematic uncertainties. Additionally, as light curves are used for the classification itself there is also a need to improve the photometry. Classification was performed using `SuperNNova` (A. Moller & T. de'Boissiere 2020),[59] using a simulated training set that includes multiple non-SN-Ia types to capture diverse sources of contamination (A. Moller et al. 2022; M. Vincenzi et al. 2023).

This work focuses on the extraction of the photometric light-curve fluxes from the 5 yr observations of the DES-SN program, and the subsequent public data release. Past cosmological analyses have long utilized two main methods for extracting SN photometry: `DiffImg` followed by point-spread function (PSF) fitting photometry on coadded difference images, and a forward modeling method called SMP. In this paper, we present the photometry measurements using both methods. The `DiffImg` photometry was produced during DES operations with the primary purpose of discovering transients. SMP was run independently of DES operations,

[59] https://github.com/supernnova/SuperNNova

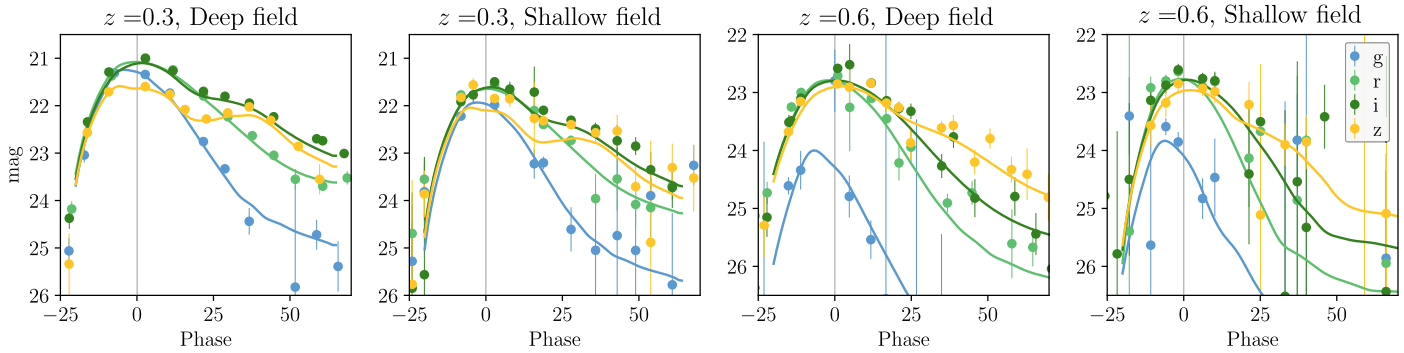

Figure 1. DES light curves of SNe at different redshifts ($z \sim 0.3$ and $z \sim 0.6$) in the SN Deep and SN Shallow fields. Lines are the SALT3 model that best fits the light-curve data.

with the purpose of obtaining high-precision photometry for the cosmology analysis; only a subset of single-season `DiffImg` candidates were able to be processed because SMP is not designed for multiseason light curves (e.g., active galactic nuclei (AGNs)). We also provide details on the ancillary data included as part of this data release.

The structure of the paper is as follows. In Section 2 we describe the photometric calibration of the images and the different photometric methods (`DiffImg` and SMP) applied to discovered transients in them. We also provide consistency checks, and describe improvements. In Section 3 we summarize the auxiliary data (redshifts, host-galaxy parameters, and photometry) provided in this release. In Section 4 we provide some concluding remarks and in the Appendix we describe the format of the data release.

2. Data

2.1. DES-SN Program Overview

The DES-SN program (M. Smith et al. 2020) ran from 2013 through 2018, spanning 5 yr and obtained images eight shallow fields: C1, C2, X1, X2, S1, S3, E1 and E2; and two deep fields: C3 and X3, in a combined footprint of $\sim$27 deg^2. The observing strategy and typical cadence, seeing and depths are provided in M. Smith et al. (2020) and E. H. J. Neilsen et al. (2019). Transients were detected before the start of the next observing evening using the `DiffImg` technique described in R. Kessler et al. (2015), and artifacts were removed using the candidate classification methodology developed in D. A. Goldstein et al. (2015). An extensive host-galaxy spectroscopic follow-up program was performed using the 2dF fiber positioner and AAOmega spectrograph on the Anglo-Australian Telescope (AAT), as part of the OzDES survey (F. Yuan et al. 2015; M. J. Childress et al. 2017; C. Lidman et al. 2020). Examples of DES-SN light curves at different redshifts in both the DES-SN Deep and Shallow fields are presented in Figure 1.

2.2. Photometric Calibration

For SN Ia cosmological measurements, it is essential to both accurately determine the interfilter calibration within a survey (especially if the survey spans a wide range of redshifts) and the intersurvey calibration (when data sets from multiple surveys are combined).

First, DES images are internally calibrated using a catalog of 17 million tertiary standard stars within the DES footprint built using the forward global calibration method (FGCM) as conceived by C. W. Stubbs & J. L. Tonry (2006) and implemented in DES by D. L. Burke et al. (2018). This method provides excellent all-sky uniformity of <3 mmag for the full DES 6 yr (Y6) dataset (I. Sevilla-Noarbe et al. 2021; E. S. Rykoff et al. 2023).

The FGCM tertiary standard star catalog provided in D. L. Burke et al. (2018) was utilized in the DES-SN3YR cosmological analysis. The FGCM catalog was updated in the period between DES-SN3YR and DES-SN5YR and here we use the stellar catalogs as presented in Appendix 3 of I. Sevilla-Noarbe et al. (2021). The improvements are summarized as follows: (i) improved corrections to aperture photometry, (ii) an update to the DES Y3A2 standard bandpasses (see I. Sevilla-Noarbe et al. 2021, Section 4.3), (iii) improved uniformity in years following the bad weather of year three (Y3; H. T. Diehl et al. 2016), (iv) improved astrometry using the longer temporal baseline, and (v) other technical and practical improvements.

SN Ia cosmology analyses, including M. Vincenzi et al. (2024), use multiple surveys to cover the low-redshift range and the high-redshift range, both needed for competitive cosmological constraints. For this reason, we utilize the calibration of D. Brout et al. (2022; Supercal-Fragilistic), which is an improvement over the D. Scolnic et al. (2015; Supercal) method. This method consists of simultaneously cross calibrating the FGCM catalog with the stellar catalogs from numerous other wide-field surveys (e.g., Pan-STARRS 1, the Sloan Digital Sky Survey (SDSS), and SNLS). The Supercal-Fragilistic methodology consists in determining a global solution that minimizes the differences between each survey by using their published calibrations as prior information. Supercal-Fragilistic finds similar sign of offsets for DES [+0.002, −0.009, −0.007, +0.006] in [g, r, i, z] as those found in E. S. Rykoff et al. (2023) [+0.001, −0.003, −0.001, +0.002], but of larger magnitude; though we find that these offsets are consistent with each other given that the external tertiary cross-calibration data used to perform the calibration in Supercal-Fragilistic is independent from E. S. Rykoff et al. (2023).

In this work we have chosen to adopt the offsets from Supercal-Fragilistic because: (1) the low-z samples used with the DES-SN5YR sample to constrain cosmology have been calibrated in Supercal-Fragilistic, (2) included is the covariance between DECam filters and low-z filters utilized in the cosmology likelihood (see Equation (11) of M. Vincenzi et al. 2024), (3) Supercal-Fragilistic provides a mechanism to create multiple realizations of interfilter correlated calibrations from the Supercal-Fragilistic covariance matrix for accurate

Table 1
Differences between DiffImg and Scene Modeling Photometry

Stages	DiffImg	SMP Y5
Template	Science verification images	Any high-quality images taken before or after transient
Catalog for Zero-point	Science verification catalog	Y6 forward model global calibration
Photometry for Zero-point	Source Extractor MAG_AUTO	PSF photometry
Tertiary Star Proper motion	None	Linear fit over 5 yr
Astrometry	Science verification	Updated in G. M. Bernstein et al. (2017)
Transient Position	Forced at average DiffImg Position across filters	Varied position per filter (common across all epochs)
Host-galaxy Profile	From DiffImgtemplate	Forward model fitted per filter
Flux Measurement	DIA + forced-PSF photometry	Forward model scene + forced-PSF photometry but with varied position across all images

survey simulations, and (4) Supercal-Fragilistic is more accurate and precise due to the utilization of more external data. The differences in tertiary standard stars between what was used in DES-SN3YR and the Y6 catalog used in this work are ∼9 mmag for $g-z$, ∼0 mmag for $g-i$, and ∼5 mmag for $g-r$.

The AB offset uncertainties reported in the analysis of E. S. Rykoff et al. (2023), based on the Hubble Space Telescope CalSpec standard star C26202, are ∼0.011 mag. The reported DES-SN5YR uncertainties (statistical + systematic) in Supercal-Fragilistic on the diagonal of the covariance matrix are half the size (6 mmag), which is the result of leveraging multiple surveys utilizing multiple primary standard stars. The full Supercal-Fragilistic covariance[60] is used to determine the effects of correlated systematic uncertainties in both light-curve fitting and in SALT3 model training. Systematic uncertainties due to absolute calibration of the DECam and low-z filters are discussed in Section 6.1 of M. Vincenzi et al. (2024).

2.3. Forced Photometry on Image Differences

The DES DiffImg pipeline obtains a first and preliminary measurement of transient fluxes using PSF photometry on images obtained as result of a difference image analysis (DIA; C. Alard & R. H. Lupton 1998; C. Alard 2000). Details of the DES implementation of DiffImg are provided in R. Kessler et al. (2015) and are also outlined in Table 1. In summary, DiffImg uses a deep template image, constructed from coadding science verification images obtained under very good observing conditions (low sky noise and small PSF size). The template image is transformed to match the image properties of the nightly observation, first by astrometric registration and then by convolution with an image kernel. The resulting difference image contains signals only in pixels where there are flux changes, either from real sources, image artifacts, or noise. The pixels with detected sources 3.5σ above the sky noise level are evaluated by a separate trained machine learning artifact rejection code (D. A. Goldstein et al. 2015).

It is important to note that the detection algorithm was performed on search images processed before the start of the next observing night, and on template images from science verification data. While this pipeline was used to discover all transients included in this data release, and to develop cosmology analysis methods (SMP; K19; M. Vincenzi et al. 2019; A. Moller et al. 2022; A. Möller et al. 2024, etc.), it has not been optimized for SN cosmology. The photometric zero-points in DiffImg were calculated from the science verification tertiary standard star catalog and thus do not make use of the updated Y6 catalogs.

Furthermore, the DiffImg pipeline has not been optimized to reduce the impact of astrometric and seeing dependent biases. The photometry of tertiary stars in the search images was carried out using Source Extractor's automatic aperture estimator (MAG_AUTO; E. Bertin & S. Arnouts 1996). However, since PSF fitting is applied to the transient in the difference images, this approach can introduce subtle biases related to magnitude, color, seeing, and airmass. Additionally, in the DiffImg pipeline there is no accounting for stellar proper motions over the course of the 5 yr survey, which results in millimagnitude photometric biases for tertiary stars with high proper motion. Finally, the location of each candidate is estimated using an average across all bandpasses, thus ignoring atmospheric effects as a function of airmass and source color (D. Brout et al. 2019a; J. Lee et al. 2023). These effects have been improved in the final photometric pipeline that leverages a technique called SMP and incorporates many of these effects both in the model itself or as corrections.

2.4. Scene Modeling Photometry

The DES SMP pipeline (D. Brout et al. 2019a, hereafter B19) was first developed for the DES-SN3YR cosmology analysis (D. Brout et al. 2019b), and in this work we applied it on the full set of 31,636 DiffImg candidates collected during the 5 yr of DES-SN operations. The resulting light-curve data set has been used for the DES-SN5YR cosmology analysis (DES Collaboration 2024; M. Vincenzi et al. 2024). Since SMP is a model-dependent fit, it is not guaranteed to converge for candidates with multiseason variability, as the model here used assumes only variability during one season for each transient and that there is zero flux during the previous and the following corresponding observing seasons; thus the total number of SMP-fitted events that we provide in the data release is 19,706. The details of the SMP method are discussed in detail in B19. In summary, SMP simultaneously forward models the DECam images of the transient and its host galaxy while accounting for atmospheric and instrumental effects.

For each transient event "search" image with a candidate detection, the SMP model is convolved with the PSF of each image as determined by PSFex (E. Bertin 2011) in Fourier space and is then resampled to match the pixel grid of the image. This results in a series of "model images" that are compared to the observed DECam images. The time series of DECam images that are used for constraining the transient

[60] https://github.com/PantheonPlusSH0ES/DataRelease

fluxes are trimmed to span the entire light curve of a transient by using an estimation of the time of peak brightness from the DiffImg light curve and allowing the transient flux to vary for images that occur within 40 days prior and 300 days after the DiffImg estimated peak. Images taken beyond this range (hereafter referred to as "reference" images) are assumed to have zero transient flux and aid in constraining the degeneracy between a point source at the location of the transient and the underlying galaxy model.

SMP presents several improvements over the DiffImg pipeline, and these are notably not limited to the methodology. There were also procedural and practical improvements that occurred over the years intervening the two separate efforts to process the data (see Table 1). For SMP, reference and search images were reprocessed through the FinalCut program (E. Morganson et al. 2018) and were scaled to a common zero-point using the updated DES Y3A2 standard bandpasses and tertiary standard stars (see I. Sevilla-Noarbe et al. 2021). The SMP pipeline also incorporates the updated astrometric solution from G. M. Bernstein et al. (2017).

The reference images for SMP are individual exposures, drawn from the highest-quality DES images taken over the course of the entire 5 yr survey. While more reference images for SMP is desirable, the SMP method computing resource use scales linearly as $O(N_{\rm References})$, and for the full 5 yr set of images there are often over 1000 potential reference images in the deep fields. We therefore require $N_{\rm References} = N_{\rm Search}$ and prioritize the templates with the best seeing (FWHM), PSF, and sky level in order to improve the convergence of the SMP galaxy model.

Unlike DiffImg (which used MAG_AUTO), the SMP pipeline does not allow the position of tertiary stars to float on each image, but rather performs forced-position PSF fitting photometry on the tertiary stars after accounting for their proper motions. SMP maintains consistency in the photometric methodology between the tertiary stars and the transient (also forced-PSF fitting photometry) and it is this consistency that is essential for mitigating biases in the calibrated transient flux (A. Rest et al. 2016). Additionally, the SMP pipeline was developed to account for the proper motion of the tertiary stars over the course of the 5 yr survey by incorporating a linear fit in R.A. and decl. to the identified single epoch centroid positions on each night. While the tertiary stars have a high SNR and thus their forced positions can be accurately measured, the transients usually have a relatively low SNR and their positions are less certain. Consequently, we incorporate the R.A. and decl. of each transient candidate into the fitted SMP model. This approach offers the added advantage of the posterior uncertainties naturally accommodating the positional uncertainty of the SN and accounting for potential photometric bias in the positional uncertainty.

Lastly, it is important to note that the SMP pipeline as implemented by B19 fits an independent model for each bandpass. This mitigates any source-color and filter-dependent atmospheric effects. Additional atmospheric corrections (such as in J. Lee et al. 2023) are minimal (see also Section 2.7).

We compare the released Y3 photometry in B19 with our more recent reprocessing (year five (Y5)) of the same SN Ia sample but with improved templates, astrometry, and tertiary catalogs. Before performing the comparison we apply offset corrections [−0.006, +0.007, +0.001, −0.005] in the corresponding [g, r, i, z] filters, to remove changes in the determination of the AB calibration over the time span in which the Y3 and Y5 data were processed. Figure 2 shows the magnitude difference between our Y5 (this work) and the Y3 (B19) SMP light-curve magnitudes after removing the AB offset differences. The median is consistent with zero for all filters and the dispersion is found to be the result of the various image processing improvements from Y3 to Y5 in combination with independent Markov Chain Monte Carlo fitting. We find for the largest magnitude residuals between Y3 and Y5 that these differences are specifically the result of the improved astrometry. The mean uncertainty on the r-band SN position for the largest residuals ($\Delta{\rm mag}_{\rm SMP} > 0.05$) is 0.08 pixels, which is smaller than the average uncertainty of the full sample (0.33 pixels). We observe small offsets in each filter and search for trends as a function of Y5-observed magnitude. Negative residuals for fainter sources are expected with improved low-flux measurements. We find small trends in all bands suggesting improved Y5 sensitivity.

2.5. Nightly Fluxes and Their Uncertainties

The DES-SN program observed 10 fields in the sky: eight shallow fields and two deep fields. Some transients are observed multiple times per night in the same filter. In these cases, we average the results (in the deep fields and z band; see Table 1 from R. Kessler et al. 2015). In the case of DiffImg, the coaddition takes place at the pixel level, by inverse variance weighted image stacking, whereas SMP examines every image as an independent data vector and obtains a flux per individual image, which is later used to calculate the light-curve epoch fluxes using again the inverse variance weighted average.

The photometric uncertainties in DiffImg are determined solely from the PSF fit procedure. The SMP photometry flux uncertainties per observation t_i are determined as follows:

$$\sigma_{t_i} = \sqrt{\sigma^2_{\rm SMP} + \sigma^2_{\rm source} + \sigma^2_{\rm hostgal}}, \quad (1)$$

where $\sigma_{\rm SMP}$ is determined from the marginalized posterior. The SMP likelihood (B19, Equation (1)) contains sky noise but also includes a nonlinear component due to uncertainty in the fitted position of the SN. Mean fitted position uncertainties for the SNe are given in Table 2. The SMP galaxy model fit from all observations is convolved with the individual night PSF to obtain the Poisson noise contribution of the host galaxy $\sigma_{\rm hostgal}$. The nightly Poisson source noise ($\sigma_{\rm source}$) is included after fits are performed following P. Astier et al. (2013).

For light-curve fitting in the cosmology analysis, nightly fluxes are estimated as the variance weighted average $f = \sum_{t_i} f_{t_i} w_{t_i} / \sum_{t_i} w_{t_i}$ with $w_{t_i} = \sigma_{t_i}^{-2}$, thus the total SMP uncertainty per epoch is $\sigma^2_{\rm stat} = 1/\sum_{t_i} w_{t_i}$.

2.6. Host Surface Brightness Anomaly Corrections

The so-called "surface brightness anomaly" (R. Kessler et al. 2015) is a systematic underestimation of flux uncertainties for SNe located in high local galaxy surface brightness regions.

In B19, it was suggested that this anomaly would be reduced with improved astrometry. We estimate the rms of flux pulls on epochs free of transient flux (i.e., the flux over the measured flux uncertainty where the true flux is zero) and plot their mean value as a function of the host-galaxy surface brightness. In Figure 3, we present our results for all bands separately, and for both for DiffImg and SMP. We see that for g band the

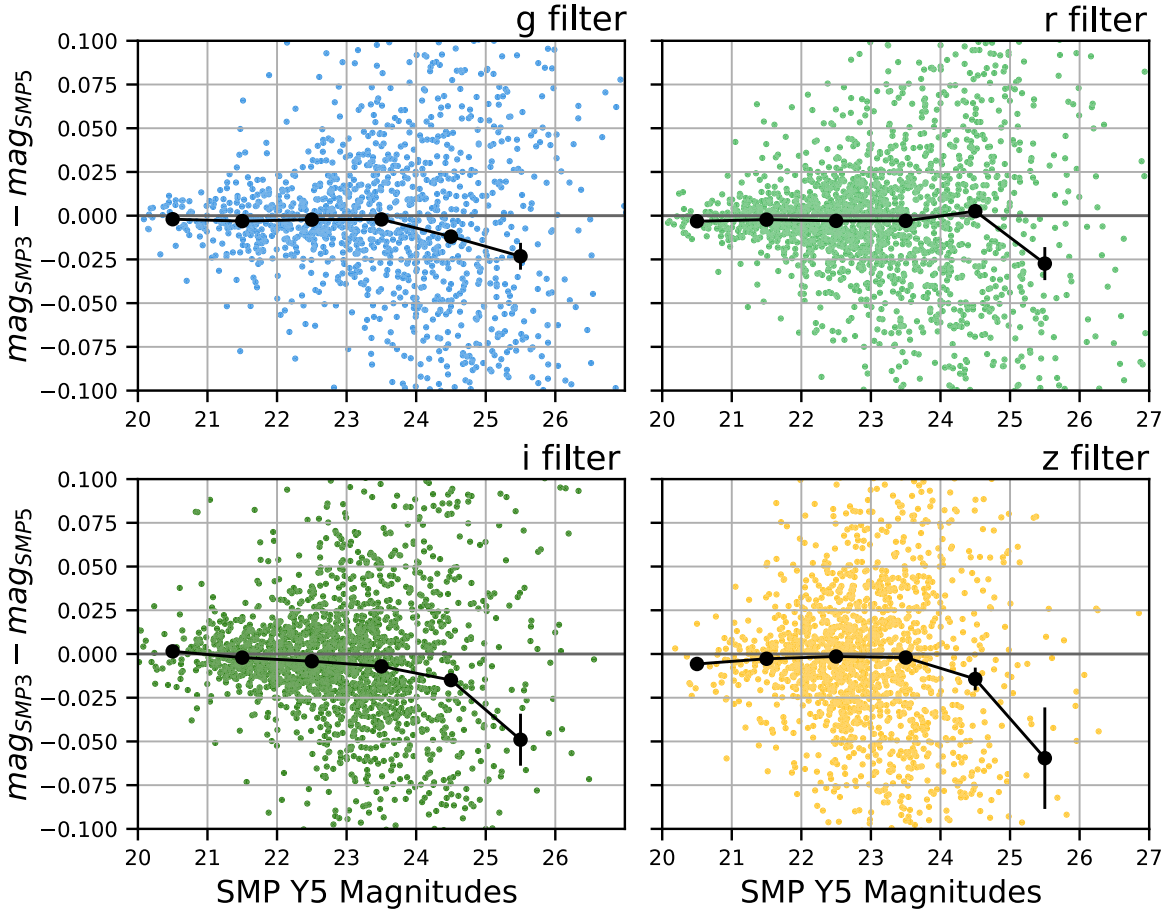

Figure 2. Difference in magnitudes for transients analyzed with SMP Y3 (B19) and SMP Y5 (this work). We expect subtle differences due to the improved catalogs, image processing and astrometry pipelines, and underlying photometric uncertainties. The trend seen in the *i* band is at 2σ significance, which is the largest out of all bands.

Table 2
Mean Uncertainty (in Pixels and in Arcseconds) on the Fitted Supernova Positions Obtained with Scene Modeling Photometry

Band	$<\sigma_{xy}>$ (px)	$<\sigma_{(\mathrm{R.A.,\ Decl.})}>$ ($''$)
g	0.43	0.12
r	0.33	0.09
i	0.31	0.08
z	0.32	0.09

surface brightness anomaly is unimportant in comparison with the redder bandpasses. For *r* and *i* bands we find that SMP clearly reduces the excess scatter although (as also in *z* band) the effect is not fully corrected. We define a scale correction *S* as the rms ($\Delta f/\sigma_{\mathrm{stat}}$), and as in B19 we scale the SMP light-curve photometric uncertainties σ_f as follows:

$$\sigma_f = \sigma_{\mathrm{stat}} \times S. \quad (2)$$

2.7. Wavelength-dependent Atmospheric Corrections

After the SMP pipeline, we perform two sets of corrections to the DES-SN photometry. These corrections are the result of wavelength-dependent atmospheric effects.

First, the wavelength-dependency of the atmospheric refractive index results in differential chromatic refraction (DCR; e.g., A. V. Filippenko 1982; M. C. Kaczmarczik et al. 2009). Second, atmospheric turbulence causes wavelength-dependent (λ-dependent) seeing variations. While these photometric biases are similar for both SN and tertiary standard star photometry, they do not cancel out due to the fact that the typical SN spectral energy distribution (SED) is bluer than the typical stellar SED.

The method to compute the expected corrections to DES-SN photometry is described in J. Lee et al. (2023). These corrections have not been applied in this data release, rather they are applied as a lookup table in the light-curve fitting process. The lookup table is provided as part of the DES-SN5YR data release (see Appendix A). The DCR and λ-dependent seeing corrections are small ($\sim$3 mmag) and J. Lee et al. (2023) assess their impact on DES-SN distance estimation and cosmological results to be minimal.

While these corrections could have been included in the SMP model or PSF model, these efforts were developed in parallel for DES and were instead chosen to be included as corrections to the reported SMP fluxes. These corrections are included as supplementary files in the data release as shown in Appendix A.

2.8. Comparison of `DiffImg` Real-time Photometry and Scene Modeling Photometry

Training the SALT3 SN Ia model can be done using public software (W. D. Kenworthy et al. 2021), and here we compare

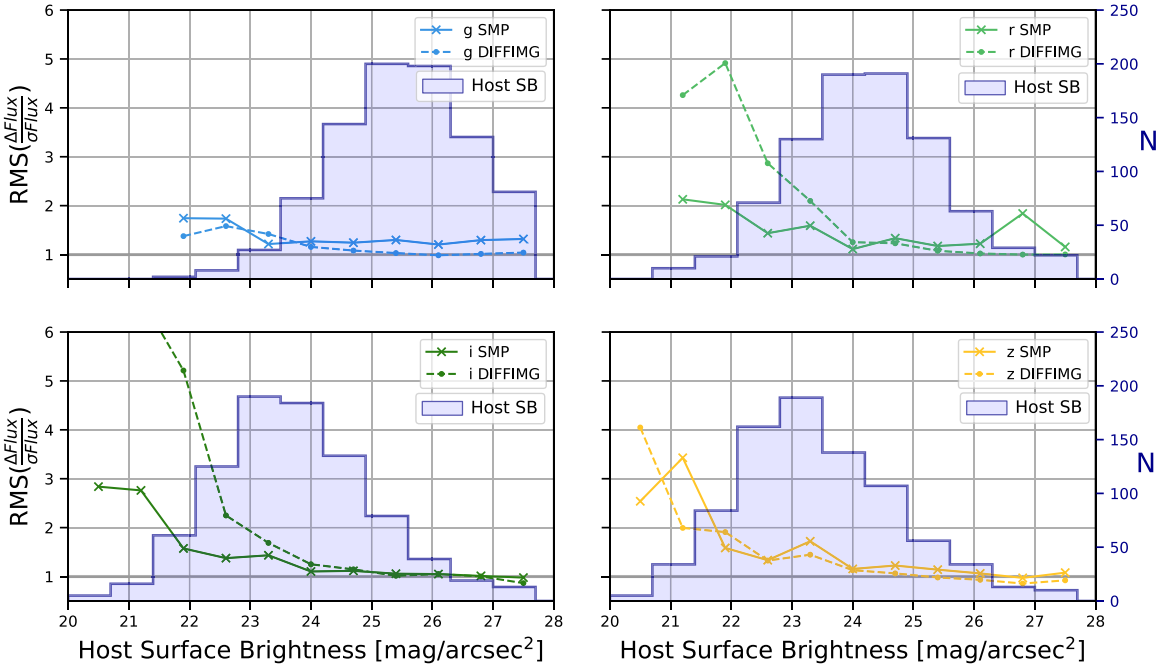

Figure 3. Rms for the flux pull on epochs free of transient flux (assuming a true flux of zero), as a function of the surface brightness of the galaxy host, exactly at the location of the transient. We include the distribution of host surface brightness for each filter in blue. The horizontal line indicates the expected rms = 1 for a unit dispersion Gaussian. We show the results for SMP (solid line) and `DiffImg` (dashed line).

SALT3 model fits for `DiffImg` and SMP, using the training described in G. Taylor et al. (2023). This training did not include DES data. The number of likely SNe Ia that comprise the "cosmological sample" is 1635, which include light-curve quality cuts and bias correction viability cuts among others, and are discussed in great detail in Table 4 of the companion paper M. Vincenzi et al. (2024).

In Figure 4, we show the light-curve model residuals to this subset of SNe for both `DiffImg` and SMP. The scatter of residuals about the SALT3 model is typically reduced in the SMP version of photometry in all bands for a wide range of redshifts (and a wide range of SNR values).

We include the total number of transients with `DiffImg` photometry that were run through SMP in Table 3. We also include the number of light curves with successful SMP chain runs in the four DES filters, and those with any three successful filters, two, and only one successful DES filter(s). We also include the number of events that pass a multiseason transient cut designed to remove AGNs and long-lived transients, and the number of events that have a classification probability of being an SN Ia ($P_{\rm SNIa} > 0.5$) obtained with the `SuperNNova` classifier (A. Moller et al. 2022). We note that not all SMP fits converge in all filters. The SMP process relies on several fundamental assumptions that if not satisfied can result in nonconvergence of the fits (e.g., the assumption of zero transient flux outside the season of the transient's peak flux). When we select the sample of events that pass the multiseason cut from A. Moller et al. (2022; i.e., are not AGNs or long-lived transients), we find that for 13,507 (96%) SMP successfully converged for at least one filter, and for 13,398 of these events (95%) SMP processes all four filters successfully. The ratio of light curves that have successful SMP convergence in all four filters relative to the number of `DiffImg` candidates is around 50%, which is consistent with the Monte Carlo simulations done in R. Kessler et al. (2015),

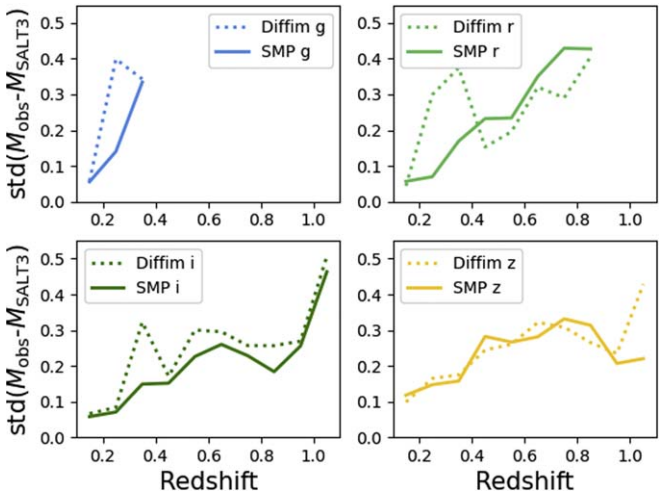

Figure 4. Comparison of flux residuals to SALT3 model fits for `DiffImg` and SMP DES-SN5YR light curves. We generally find a smaller amount of residual scatter for the SMP photometry in transients across the full redshift range.

which predicted 75% of the `DiffImg` candidates are not in fact SNe, and 45% are not single epoch artifacts. When selecting events with probability scores $P_{\rm SNIa} > 0.5$ we find that for 4728 (92%) of the events have successful SMP fits in at least one filter, and for 4702 (91%) events have successful SMP fits with all four filters.

In Table 3 we also show the number of events that pass the cuts related to the cosmology analysis from M. Vincenzi et al. (2024), including events for which DES obtained host-galaxy redshift information and also pass the conventional SALT3 model parameter cuts, and final Hubble diagram (HD) quality cuts. This shows that SMP delivers photometry measurements with higher quality, which ultimately increases the size of the DES-SN5YR cosmology sample.

Table 3
Number of Transients Processed with the DiffImg and Scene Modeling Photometry Pipelines

# Filters	Total	4	3	2	1	Multiseason Cut	$P_{\rm SNIa} > 0.5$	With Host z and SALT3 Fit	H. Quality Cut
# DiffImg Light Curves	31,636	31,636	⋯	⋯	⋯	14,068	5153	4032	1499
# SMP Light Curves	19,706	14,486	4179	702	339	13,507	4728	3621	1635

3. Auxiliary Data

3.1. DES-SN Redshifts

For each SN, we identify the host galaxy using the directional light radius method presented by M. Sullivan et al. (2010). The galaxies identified as likely hosts of DES transients are targeted using the AAOmega spectrograph on the 3.9 m AAT as part of the OzDES program (F. Yuan et al. 2015; M. J. Childress et al. 2017; C. Lidman et al. 2020). A full description of the different sources of redshifts used in our sample and the spectroscopic efficiency of the OzDES + external catalogs are presented by M. Vincenzi et al. (2021) and B19.

3.2. DES-SN Host-galaxy Properties

Galaxy properties of DES-SN hosts are measured using DES broadband photometry and, when available, *u*-band data from SDSS and *JHK* data from VISTA[61] (W. Sutherland et al. 2015).

DES broadband photometry is measured from the DEEP coadds presented by P. Wiseman et al. (2020). We use the galaxy SED fitting code by M. Sullivan et al. (2010) and the PÉGASE2 galaxy spectral templates of M. Fioc & B. Rocca-Volmerange (1997) and D. Le Borgne & B. Rocca-Volmerange (2002), assuming a P. Kroupa (2001) initial mass function. The fraction of potentially mismatched SN hosts is modeled and studied in detail by H. Qu et al. (2024) and all identified potential host galaxies are included in the data release.

3.3. Low-z Redshifts

For the low-z SNe, we use the spectroscopic redshifts revised by A. Carr et al. (2022) and corrected for peculiar velocities by E. R. Peterson et al. (2022). These peculiar velocity corrections are based on the 2M++ density fields (J. Carrick et al. 2015) with the global parameters found in K. Said et al. (2020), combined with the group velocities estimated from R. B. Tully (2015). We consider the uncertainties on the peculiar velocity estimates to be 240 km s^{-1}.

3.4. Low-z Host-galaxy Properties

For the low-redshift sample, we use the same SED fitting code and assumptions implemented to measure the host-galaxy properties in the DES sample. Low-z optical photometry is combined with near-ultraviolet photometry from SDSS *u*-band images and the Galaxy Evolution Explorer. This ensures coverage in rest-frame *u* band, essential to reliably determine the $u - r$ rest-frame color.

We remeasure all the optical and near-ultraviolet low-z host-galaxy photometry using the open-source package hostphot (T. E. Muller-Bravo & L. Galbany 2022).[62] We measure the global galaxy photometry and visually inspect every SN host-galaxy photometric measurement to ensure that the selected aperture is correct.

4. Conclusion

We introduce the DES-SN5YR light-curve sample, obtained with the SMP photometric technique. This sample constitutes the largest collection of SN-like transient light curves up to $z \sim 1$ obtained with a single instrument. This sample significantly improves on the quality of the photometry measurement with respect to forced-PSF photometry on DiffImg images by leveraging advances in survey calibration, star proper motion modeling, adequate calibration star PSF photometry, mitigation of atmospheric chromatic effects and source-color effects, among others. We also find a reduction on the surface brightness anomalous scatter effect in SMP with respect to DiffImg photometry. The light-curve fluxes are consistent with the previous-released DES-SN3YR sample, after accounting for zero-point offsets.

This data set of SN Ia light curves is used in M. Vincenzi et al. (2024) and DES Collaboration (2024) to obtain the most accurate constraints on the parameters of the current standard model of cosmology to date. The DES-SN5YR data set provides an independent measurement of the accelerated expansion of the Universe and paves the way for the next-generation (Stage IV) cosmological probes with the Vera Rubin Observatory Legacy Survey of Space and Time and the future space-based Nancy Grace Roman Survey Telescope. We note that the SMP pipeline performed here consumed roughly 6 million CPU hours for our 20,000 candidates in DES. Future experiments will need to leverage speed improvements available in recent differentiable models, or GPU computing developments to run on the millions of events expected in the next decade.

Acknowledgments

Funding for the DES Projects has been provided by the U.S. Department of Energy, the U.S. National Science Foundation, the Ministry of Science and Education of Spain, the Science and Technology Facilities Council of the United Kingdom, the Higher Education Funding Council for England, the National Center for Supercomputing Applications at the University of Illinois at Urbana-Champaign, the Kavli Institute of Cosmological Physics at the University of Chicago, the Center for Cosmology and Astro-Particle Physics at the Ohio State University, the Mitchell Institute for Fundamental Physics and Astronomy at Texas A&M University, Financiadora de Estudos e Projetos, Fundação Carlos Chagas Filho de Amparo à Pesquisa do Estado do Rio de Janeiro, Conselho Nacional de Desenvolvimento Científico e Tecnológico and the Ministério da Ciência, Tecnologia e Inovação, the Deutsche Forschungsgemeinschaft, and the Collaborating Institutions in the Dark Energy Survey.

[61] The additional *uJHK* photometry is available for the C3, X3, E2. To evaluate the impact of near-infrared data in our fits, we measure host masses and $u - r$ rest-frame colors with and without *uJHK* photometry and do not find any significant bias across the full DES redshift range.
[62] https://github.com/temuller/hostphot

The Collaborating Institutions are Argonne National Laboratory, the University of California at Santa Cruz, the University of Cambridge, Centro de Investigaciones Energéticas, Medioambientales y Tecnológicas-Madrid, the University of Chicago, University College London, the DES-Brazil Consortium, the University of Edinburgh, the Eidgenössische Technische Hochschule (ETH) Zürich, Fermi National Accelerator Laboratory, the University of Illinois at Urbana-Champaign, the Institut de Ciències de l'Espai (IEEC/CSIC), the Institut de Física d'Altes Energies, Lawrence Berkeley National Laboratory, the Ludwig–Maximilians Universität München and the associated Excellence Cluster Universe, the University of Michigan, NSF's NOIRLab, the University of Nottingham, The Ohio State University, the University of Pennsylvania, the University of Portsmouth, SLAC National Accelerator Laboratory, Stanford University, the University of Sussex, Texas A&M University, and the OzDES Membership Consortium.

Based in part on observations at Cerro Tololo Inter-American Observatory at NSF's NOIRLab (NOIRLab Prop. ID 2012B-0001; PI: J. Frieman), which is managed by the Association of Universities for Research in Astronomy (AURA) under a cooperative agreement with the National Science Foundation.

Based in part on data acquired at the Anglo-Australian Telescope. We acknowledge the traditional custodians of the land on which the AAT stands, the Gamilaraay people, and pay our respects to elders past and present. Parts of this research were supported by the Australian Research Council, through project numbers CE110001020, FL180100168, and DE230100055. Based in part on observations obtained at the international Gemini Observatory, a program of NSF's NOIRLab, which is managed by the Association of Universities for Research in Astronomy (AURA) under a cooperative agreement with the National Science Foundation on behalf of the Gemini Observatory partnership: the National Science Foundation (United States), National Research Council (Canada), Agencia Nacional de Investigación y Desarrollo (Chile), Ministerio de Ciencia, Tecnología e Innovación (Argentina), Ministério da Ciência, Tecnologia, Inovações e Comunicações (Brazil), and Korea Astronomy and Space Science Institute (Republic of Korea). This includes data from programs (GN-2015B-Q-10, GN-2016B-LP-10, GN-2017B-LP-10, GS-2013B-Q-45, GS-2015B-Q-7, GS-2016B-LP-10, GS-2016B-Q-41, and GS-2017B-LP-10; PI: Foley). Some of the data presented herein were obtained at Keck Observatory, which is a private 501(c)3 nonprofit organization operated as a scientific partnership among the California Institute of Technology, the University of California, and the National Aeronautics and Space Administration (PIs: Foley, Kirshner, and Nugent). The Observatory was made possible by the generous financial support of the W. M. Keck Foundation. This paper includes results based on data gathered with the 6.5 m Magellan Telescopes located at Las Campanas Observatory, Chile (PI: Foley), and the Southern African Large Telescope (SALT; PIs: M. Smith and E. Kasai).

The DES data management system is supported by the National Science Foundation under grant Nos. AST-1138766 and AST-1536171. The DES participants from Spanish institutions are partially supported by MICINN under grants ESP2017-89838, PGC2018-094773, PGC2018-102021, SEV-2016-0588, SEV-2016-0597, and MDM-2015-0509, some of which include ERDF funds from the European Union. IFAE is partially funded by the CERCA program of the Generalitat de Catalunya. Research leading to these results has received funding from the European Research Council under the European Union's Seventh Framework Program (FP7/2007-2013) including ERC grant agreements 240672, 291329, and 306478. We acknowledge support from the Brazilian Instituto Nacional de Ciência e Tecnologia (INCT) do e-Universo (CNPq grant 465376/2014-2).

This manuscript has been authored by Fermi Research Alliance, LLC under Contract No. DE-AC02-07CH11359 with the U.S. Department of Energy, Office of Science, Office of High Energy Physics.

This research used resources of the National Energy Research Scientific Computing Center (NERSC), a U.S. Department of Energy Office of Science User Facility located at Lawrence Berkeley National Laboratory, operated under Contract No. DE-AC02-05CH11231 using NERSC award HEP-ERCAP0023923.

We acknowledge the University of Chicago's Research Computing Center for their support of this work.

Contribution Statements

Author contributions are as follows. Paper writing: B.O.S., D.B., and M.V. Data processing: B.O.S., K.H., D.B., and M.Sa. Data validation: B.O.S., D.B., R.K., M.V., and M.Sa. Code development: D.B., B.O.S., M.Sa., R.K., and P.A. Contributed to ancillary data products: A.M., H.Q., M.Sm., M.Su., P.W., M.Sa., R.Ch., D.B., M.V., C.L., L.G., R.Ke., S.H., J.L., M.A., and B.O.S. Working group leadership: T.D. and D.S. Other DES SNWG people contributed to the interpretation and analysis of the data and provided comments on the manuscript. The remaining authors have made contributions to this paper that include, but are not limited to, the construction of DECam and other aspects of collecting the data; data processing and calibration; developing broadly used methods, codes, and simulations; running the pipelines and validation tests; and promoting the science analysis.

Appendix
Data Release Details

We provide `DiffImg` photometry for 31,636 candidates, SMP photometry for 19,706 candidates, and ancillary data at github.com/des-science/DES-SN5YR and doi:10.5281/zenodo.1272077.

For the SMP light curves, we provide the following metadata.

1. `REDSHIFT`. Determined from the host galaxy using OzDES and other external catalogs.
2. `HOST_g/r/i/z`. Determined from deep coadded DES images (P. Wiseman et al. 2020).
3. `HOST_LOGMASS` and `HOST_COLOR`. Host stellar mass and $u-r$ rest-frame color, determined as described in Section 3.2.

We also provide the following time-series data.

1. `MJD`. Modified Julian Date of the light-curve data.
2. `ZPT`. Redetermination of the zero-point of the image for SMP scaling.
3. `BAND`. DES filter.
4. `SKY`. Sky level in units of image counts.

5. PSF. FWHM of the PSF in units of arcseconds.
6. FLUXCAL. Reported SMP flux in units of *fluxcal counts* (fixed standard zero-point of 27.5).
7. FLUXCALERR. Reported SMP flux uncertainty in units of *fluxcal counts*.

For the low-z sample, we release the updated host-galaxy photometry and properties.

1. HOST_NUV/u/g/r/i/z. Determined from P. Wiseman et al. (2020).
2. HOST_LOGMASS and HOST_COLOR. Host stellar mass and $u-r$ rest-frame color, determined as described in Section 3.2.

Additional corrections:

1. DCR Correction (J. Lee et al. 2023) lookup table.

A.1. Light-curve Example

An example light curve in text format is included for general reference.

```
SURVEY:    DES
SNID:    1246273
SNTYPE:    0
FAKE:    0
FILTERS:    griz
NXPIX:    2048
NYPIX:    4096
PIXSIZE:    0.263000
RA:    54.566567
DEC:    -27.994892
REDSHIFT_HELIO:    2.352000 +- 0.001000
FIELD:    C1

HOSTGAL_NMATCH:    1
HOSTGAL_NMATCH2:    1
HOSTGAL_OBJID:    590
HOSTGAL_SPECZ:    2.352000 +- 0.001000
HOSTGAL_SNSEP:    0.0729999989271164
HOSTGAL_DDLR:    0.11299999803304672
HOSTGAL_RA:    54.566578
HOSTGAL_DEC:    -27.994910
HOSTGAL_MAG: 22.800 22.830 22.600 22.110
HOSTGAL_MAGERR: 0.010 0.010 0.010 0.010
HOSTGAL_SB_FLUXCAL: 15.530 12.930 18.200 29.040

# computed quantities
REDSHIFT_CMB:    2.350790 +- 0.001000
MWEBV:    0.010100 +- 0.001700
PEAKMJD:    56552.26953125
MJD_DETECT_FIRST:    56538.365000
MJD_DETECT_LAST:    -9.0

HOSTGAL_PHOTOZ:    -999 +- -999
HOSTGAL_LOGMASS:    10.656000 +- 0.019000
HOSTGAL2_PHOTOZ:    -999 +- -999
HOSTGAL2_LOGMASS:    -999 +- -9
VPEC:    0.000000 +- 300.000000

# PRIVATE (non-standard) variables
PRIVATE(DES_numepochs_ml_Y1):    28
PRIVATE(DES_numepochs_ml_Y2):    0
PRIVATE(DES_numepochs_ml_Y3):    12
PRIVATE(DES_numepochs_ml_Y4):    32
PRIVATE(DES_numepochs_ml_Y5):    16
PRIVATE(AGN_SCAN):    -1

# sim/truth quantities
SIM_TYPE_INDEX:    -9

# ----------51 # obs info
```

```
NOBS: 71
NVAR: 14

VARLIST: MJD BAND FIELD PHOTFLAG XPIX YPIX CCDNUM IMGNUM GAIN FLUXCAL FLUXCALERR PSF_SIG1 ZEROPT SKY_SIG
OBS: 56534.2230 i C1 14336 776.9 1361.6 62 228748 3.770 5.4924e+01 8.7440e+00 2.2620 32.280 20.30
OBS: 56534.2250 z C1 14336 779.5 1355.6 62 228749 4.050 8.2914e+01 1.0723e+01 2.2470 32.899 42.80
OBS: 56538.3700 i C1 13312 778.5 1291.1 62 230181 3.740 7.1572e+01 6.8920e+00 2.5070 32.601 20.80
OBS: 56538.3720 z C1 13312 786.0 1295.1 62 230182 4.080 7.5552e+01 8.2890e+00 2.4130 33.032 38.40
...
OBS: 56607.0620 z C1 12288 710.3 1289.3 62 252746 4.050 5.88 84e+01 1.4748e+01 3.4040 32.928 45.60
OBS: 56614.0730 g C1 12288 724.3 1326.2 62 255449 4.380 6.9555e+01 1.9029e+01 1.9910 32.223 38.40
OBS: 56614.0780 i C1 12288 710.0 1313.5 62 255451 3.900 5.1747e+01 8.9140e+00 1.6640 32.579 39.60
OBS: 56614.0800 z C1 12288 718.3 1310.7 62 255452 4.070 6.8474e+01 8.1760e+00 1.5850 33.046 58.20
OBS: 56615.0960 g C1 12288 726.1 1342.4 62 255888 4.330 5.3188 e+01 1.9439e+01 2.1090 32.015 36.80
OBS: 56615.1010 i C1 12288 711.0 1360.6 62 255890 3.830 5.2356e+01 9.5250e+00 1.8340 32.560 36.20
OBS: 56615.1040 z C1 12288 718.8 1367.2 62 255891 4.020 5.6826e+01 1.1180e+01 1.9620 32.996 52.80
OBS: 56628.0800 i C1 12288 718.9 1312.5 62 259320 3.820 3.6911e+01 6.0560e+00 2.1850 32.554 21.00
OBS: 56628.0830 z C1 12288 719.6 1304.5 62 259321 4.060 4.8195e+01 8.7390e+00 2.3730 33.042 41.30
OBS: 56635.1270 g C1 12288 735.5 1342.8 62 261961 4.230 5.3322e+01 5.0210e+00 2.6680 32.353 11.10
OBS: 56635.1320 i C1 12288 734.6 1360.7 62 261963 3.780 3.1282e+01 6.5190e+00 2.1480 32.605 24.40
OBS: 56635.1350 z C1 12288 726.1 1331.3 62 261964 4.060 5.2199e+01 7.6440e+00 1.8760 33.084 49.10
OBS: 56642.0880 i C1 1 785.9 1334.0 62 265092 3.360 1.5130e+02 5.8947e+01 2.3770 32.201 70.80
OBS: 56642.0900 z C1 1 770.6 1324.0 62 265093 4.020-1.9340e+00 1.8025e+01 2.0710 32.776 72.00
OBS: 56645.0780 g C1 12288 718.7 1326.5 62 266113 4.320 4.9523e+01 1.0656e+01 2.3580 32.331 24.30
OBS: 56645.0820 i C1 12288 736.7 1331.3 62 266115 3.840 4.8745e+01 7.5700e+00 1.9830 32.574 29.70
...
OBS: 56693.0340 g C1 12288 736.9 1328.8 62 281587 4.260 2.1540e+01 5.0830e+00 2.1580 32.253 13.00
OBS: 56693.0390 i C1 12288 749.5 1346.6 62 281589 3.780 2.6410e+01 6.3810e+00 1.8870 32.529 24.90
OBS: 56693.0410 z C1 12288 742.8 1354.2 62 281590 4.070 3.3742e+01 7.8600e+00 1.8980 32.982 44.70
END:
```

A.2. Structure of the Data Release

The structure of the full data release contents is summarized in Table 4.

Table 4
Structure of the DES-SN5YR Data Release

Folder	Description
0_DATA	DES-SN5YR light curves from this work, for all SN candidates that have a spectroscopic redshift and pass the light-curve quality cuts.
1_SIMULATIONS	Set of 25 SNANA simulations with the same properties as the DES-SN sample, used in the analysis for testing and cosmological analysis validation.
2_LCFIT_MODEL	SALT3 light-curve model SED time series, used for fitting the DES-SN and low-z data and all simulated samples.
3_CLASSIFICATION	Classification probabilities from the various classification algorithms used in the analysis. These include SuperNNova, SCONE, and SNIRF classifications for the HD events and SuperNNova classifications from A. Möller et al. (2024).
4_DISTANCES_COVMAT	SN distance moduli measured after bias corrections and correcting for contamination. This includes all the beams with bias correction input files used to reproduce the HD. N_{SN}-dimensional systematic covariance matrices (statistical only and statistical + systematic for all systematics combined, and also individual systematic matrices).
6_DCR_CORRECTIONS	Wavelength-dependent photometric corrections.
5_COSMOLOGY	Chains and resulting cosmological constraints for the different models presented in DES Collaboration (2024).
7_PIPPIN_FILES	This folder includes the Pippin input files needed to reproduce the DES simulations and cosmological analysis.

ORCID iDs

B. O. Sánchez https://orcid.org/0000-0002-8687-0669
D. Brout https://orcid.org/0000-0001-5201-8374
M. Vincenzi https://orcid.org/0000-0001-8788-1688
M. Sako https://orcid.org/0000-0003-2764-7093
K. Herner https://orcid.org/0000-0001-6718-2978
R. Kessler https://orcid.org/0000-0003-3221-0419
T. M. Davis https://orcid.org/0000-0002-4213-8783
D. Scolnic https://orcid.org/0000-0002-4934-5849
M. Acevedo https://orcid.org/0000-0002-5389-7961
J. Lee https://orcid.org/0000-0001-6633-9793
A. Möller https://orcid.org/0000-0001-8211-8608
H. Qu https://orcid.org/0000-0003-1899-9791
P. Armstrong https://orcid.org/0000-0003-1997-3649
B. Rose https://orcid.org/0000-0002-1873-8973
C. Lidman https://orcid.org/0000-0003-1731-0497
B. Popovic https://orcid.org/0000-0002-8012-6978
M. Smith https://orcid.org/0000-0002-3321-1432
P. Shah https://orcid.org/0000-0002-8000-6642
M. Sullivan https://orcid.org/0000-0001-9053-4820
M. Toy https://orcid.org/0000-0001-6882-0230
S. Allam https://orcid.org/0000-0002-7069-7857
J. Annis https://orcid.org/0000-0002-0609-3987
D. Brooks https://orcid.org/0000-0002-8458-5047
A. Carnero Rosell https://orcid.org/0000-0003-3044-5150
J. Carretero https://orcid.org/0000-0002-3130-0204
F. J. Castander https://orcid.org/0000-0001-7316-4573
S. Desai https://orcid.org/0000-0002-0466-3288
H. T. Diehl https://orcid.org/0000-0002-8357-7467
B. Flaugher https://orcid.org/0000-0002-2367-5049
J. Frieman https://orcid.org/0000-0003-4079-3263
J. García-Bellido https://orcid.org/0000-0002-9370-8360
E. Gaztanaga https://orcid.org/0000-0001-9632-0815
G. Giannini https://orcid.org/0000-0002-3730-1750
G. Gutierrez https://orcid.org/0000-0003-0825-0517
K. Honscheid https://orcid.org/0000-0002-6550-2023
D. J. James https://orcid.org/0000-0001-5160-4486
K. Kuehn https://orcid.org/0000-0003-0120-0808
O. Lahav https://orcid.org/0000-0002-1134-9035
G. F. Lewis https://orcid.org/0000-0003-3081-9319
H. Lin https://orcid.org/0000-0002-7825-3206
J. L. Marshall https://orcid.org/0000-0003-0710-9474
J. Mena-Fernández https://orcid.org/0000-0001-9497-7266
R. Miquel https://orcid.org/0000-0002-6610-4836
R. L. C. Ogando https://orcid.org/0000-0003-2120-1154
A. Palmese https://orcid.org/0000-0002-6011-0530
A. Pieres https://orcid.org/0000-0001-9186-6042
A. A. Plazas Malagón https://orcid.org/0000-0002-2598-0514
A. K. Romer https://orcid.org/0000-0002-9328-879X
E. Sanchez https://orcid.org/0000-0002-9646-8198
D. Sanchez Cid https://orcid.org/0000-0003-3054-7907
I. Sevilla-Noarbe https://orcid.org/0000-0002-1831-1953
E. Suchyta https://orcid.org/0000-0002-7047-9358
G. Tarle https://orcid.org/0000-0003-1704-0781
D. L. Tucker https://orcid.org/0000-0001-7211-5729
A. R. Walker https://orcid.org/0000-0002-7123-8943

References

Abbott, T. M. C., Allam, S., Andersen, P., et al. 2019, ApJL, 872, L30
Alard, C. 2000, A&AS, 144, 363
Alard, C., & Lupton, R. H. 1998, ApJ, 503, 325
Armstrong, P., Qu, H., Brout, D., et al. 2023, PASA, 40, e038
Astier, P., El Hage, P., Guy, J., et al. 2013, A&A, 557, A55
Bernstein, G. M., Armstrong, R., Plazas, A. A., et al. 2017, PASP, 129, 074503
Bertin, E. 2011, in ASP Conf. Ser. 442, Astronomical Data Analysis Software and Systems XX, ed. I. N. Evans (San Francisco, CA: ASP), 435
Bertin, E., & Arnouts, S. 1996, A&AS, 117, 393
Brout, D., Hinton, S. R., & Scolnic, D. 2021, ApJL, 912, L26
Brout, D., Sako, M., Scolnic, D., et al. 2019a, ApJ, 874, 106
Brout, D., Scolnic, D., Kessler, R., et al. 2019b, ApJ, 874, 150
Brout, D., Taylor, G., Scolnic, D., et al. 2022, ApJ, 938, 111
Burke, D. L., Rykoff, E. S., Allam, S., et al. 2018, AJ, 155, 41
Carr, A., Davis, T. M., Scolnic, D., et al. 2022, PASA, 39, e046
Carrick, J., Turnbull, S. J., Lavaux, G., & Hudson, M. J. 2015, MNRAS, 450, 317
Childress, M. J., Lidman, C., Davis, T. M., et al. 2017, MNRAS, 472, 273
DES Collaboration 2024, arXiv:2401.02929
Diehl, H. T., Neilsen, E., Gruendl, R., et al. 2016, Proc. SPIE, 9910, 458
Filippenko, A. V. 1982, PASP, 94, 715
Fioc, M., & Rocca-Volmerange, B. 1997, A&A, 326, 950
Flaugher, B., Diehl, H. T., Honscheid, K., et al. 2015, AJ, 150, 150
Goldstein, D. A., D'Andrea, C. B., Fischer, J. A., et al. 2015, AJ, 150, 82
Hinton, S., & Brout, D. 2020, JOSS, 5, 2122
Kaczmarczik, M. C., Richards, G. T., Mehta, S. S., & Schlegel, D. J. 2009, AJ, 138, 19
Kelsey, L., Sullivan, M., Smith, M., et al. 2021, MNRAS, 501, 4861
Kelsey, L., Sullivan, M., Wiseman, P., et al. 2023, MNRAS, 519, 3046
Kenworthy, W. D., Jones, D. O., Dai, M., et al. 2021, ApJ, 923, 265
Kessler, R., Bernstein, J. P., Cinabro, D., et al. 2009, PASP, 121, 1028
Kessler, R., Brout, D., D'Andrea, C. B., et al. 2019, MNRAS, 485, 1171
Kessler, R., Marriner, J., Childress, M., et al. 2015, AJ, 150, 172
Kessler, R., Vincenzi, M., & Armstrong, P. 2023, ApJL, 952, L8
Kroupa, P. 2001, MNRAS, 322, 231
Lasker, J., Kessler, R., Scolnic, D., et al. 2019, MNRAS, 485, 5329
Le Borgne, D., & Rocca-Volmerange, B. 2002, A&A, 386, 446
Lee, J., Acevedo, M., Sako, M., et al. 2023, AJ, 165, 222
Lidman, C., Tucker, B. E., Davis, T. M., et al. 2020, MNRAS, 496, 19
Moller, A., & de Boissiére, T. 2020, MNRAS, 491, 4277
Moller, A., Smith, M., Sako, M., et al. 2022, MNRAS, 514, 5159
Möller, A., Wiseman, P., Smith, M., et al. 2024, MNRAS, 533, 2073
Morganson, E., Gruendl, R. A., Menanteau, F., et al. 2018, PASP, 130, 074501
Muller-Bravo, T. E., & Galbany, L. 2022, JOSS, 7, 4508
Neilsen, E. H. J., Annis, J., Diehl, H. T., et al. 2019, arXiv:1912.06254
Perlmutter, S., Aldering, G., Goldhaber, G., et al. 1999, ApJ, 517, 565
Peterson, E. R., Kenworthy, W. D., Scolnic, D., et al. 2022, ApJ, 938, 112
Qu, H., Sako, M., Vincenzi, M., et al. 2024, ApJ, 964, 134
Rest, A., Hilbert, B., Leisenring, J. M., et al. 2016, Proc. SPIE, 9904, 99045U
Riess, A. G., Filippenko, A. V., Challis, P., et al. 1998, AJ, 116, 1009
Rykoff, E. S., Tucker, D. L., Burke, D. L., et al. 2023, arXiv:2305.01695
Said, K., Colless, M., Magoulas, C., Lucey, J. R., & Hudson, M. J. 2020, MNRAS, 497, 1275
Scolnic, D., Casertano, S., Riess, A., et al. 2015, ApJ, 815, 117
Sevilla-Noarbe, I., Bechtol, K., Kind, M. C., et al. 2021, ApJS, 254, 24
Smith, M., D'Andrea, C. B., Sullivan, M., et al. 2020, AJ, 160, 267
Smith, M., Sullivan, M., Wiseman, P., et al. 2020, MNRAS, 494, 4426
Stubbs, C. W., & Tonry, J. L. 2006, ApJ, 646, 1436
Sullivan, M., Conley, A., Howell, D. A., et al. 2010, MNRAS, 406, 782
Sutherland, W., Emerson, J., Dalton, G., et al. 2015, A&A, 575, A25
Taylor, G., Jones, D. O., Popovic, B., et al. 2023, MNRAS, 520, 5209
Tully, R. B. 2015, AJ, 149, 171
Vincenzi, M., Brout, D., Armstrong, P., et al. 2024, arXiv:2401.02945
Vincenzi, M., Sullivan, M., Firth, R. E., et al. 2019, MNRAS, 489, 5802
Vincenzi, M., Sullivan, M., Graur, O., et al. 2021, MNRAS, 505, 2819
Vincenzi, M., Sullivan, M., Moller, A., et al. 2023, MNRAS, 518, 1106
Wiseman, P., Smith, M., Childress, M., et al. 2020, MNRAS, 495, 4040
Yuan, F., Lidman, C., Davis, T. M., et al. 2015, MNRAS, 452, 3047